A world of reality—Designing land 3D programs for signal, noise, and prestack migration

Part 1 of a 2-part tutorial

NORM COOPER, Mustagh Resources, Calgary, Alberta, Canada

In this approach to 3D seismic survey design, I will say little about bin size and fold because these two concepts can detract from more important issues in 3D survey design. Focusing on fold and bin size for their own sake can often inhibit thinking more broadly about the concepts of imaging and signal versus noise qualities of a seismic program.

The technical emphasis will be on trace density and statistical diversity. Since we live in a very real world where any type of "ideal" model is likely to be distorted during implementation, we are also concerned with robustness under perturbation. I hope that all companies in the seismic data acquisition business will also want to minimize environmental impact and I know that all will be aware of survey costs. Since these last two considerations will influence a survey's source and receiver layout, they must weigh into our choice of design type and parameters.

This article, the first part of a two-part tutorial, will review methods of estimating signal and understanding noise in a given project area, discuss the concepts of trace density and statistical diversity, address concepts in prestack migration, and review the concept of bin size. One example of the misleading nature of the concept of fold will be shown to underscore the importance of diversity. The second part of this tutorial—to be published in December's *TLE*—begins with a brief discussion of the merits of various model types, which will lead to a discussion of robustness during implementation. I will suggest a data simulation method to evaluate the characteristics of a design.

Estimating signal. One of the first concerns when designing a survey is to identify the nature of the key targets to be imaged. In particular, we are generally interested in the useable offsets, wavefield complexity (shortest apparent wavelengths required), and relative signal strength. These should be considered for all significant reflections used in the interpretation of the target prospect. We should also consider targets that may be of importance to other users of the data both now and in the future.

Often, we use simple calculations to estimate these factors. Such calculations should be used as guidelines only. Figure 1 shows one example of the results of such calculations. (The equations used are summarized in the appendix.) By using estimates of refraction and direct wave velocities, two-way traveltimes and stacking velocities for a series of reflectors, we can estimate the maximum useable offset beyond which first break mutes and/or stretch mutes limit the use of far-offset data.

For more complex models, these values are better obtained by more sophisticated modeling such as elastic wave equation models. I prefer to use modern wave equation modeling rather than ray tracing as it yields much more trustworthy information and PC versions of such software are now quick and affordable. Figure 2 is one example.

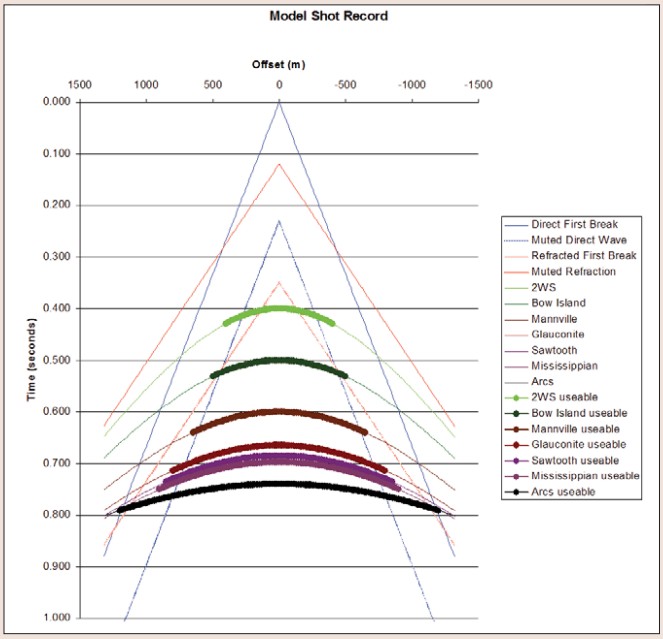

Figure 1. *Calculated useable offsets for a project in SW Alberta.*

Of course, the best source of such signal information is existing data from the area. Shot records, common offset stacks, and past processor's mutes should all be reviewed if older data are available. One problem with this method is that older 2D data may not have been recorded with sufficient offsets to adequately define maximum useable offsets. Then we have to supplement our information with the calculation and modeling methods.

Types of noise. The nature of noise in seismic data must be understood if we are to successfully design 3D seismic programs. The basic assumption that noise is random is very limited. Noise, like most seismic attributes, can be regarded as a function of several variables including time of day (t), source location (s), receiver location (r), source receiver offset (x), and source receiver azimuth (alpha):

$$Noise = F(t,s,r,x,alpha)$$

To assume that noise is random is to state that noise is time variant. Random noise observed by a spread of receivers around one source point should be different if that source point is repeated at a different time. Examples of such noise include cultural noise, traffic noise, and wind noise.

Consider the two records in Figure 3. Most geophysicists would agree that these records appear to contain a high level of "random" noise. However, a close examination will show that, although they were recorded at different times, the noise is identical in most areas. Only a few

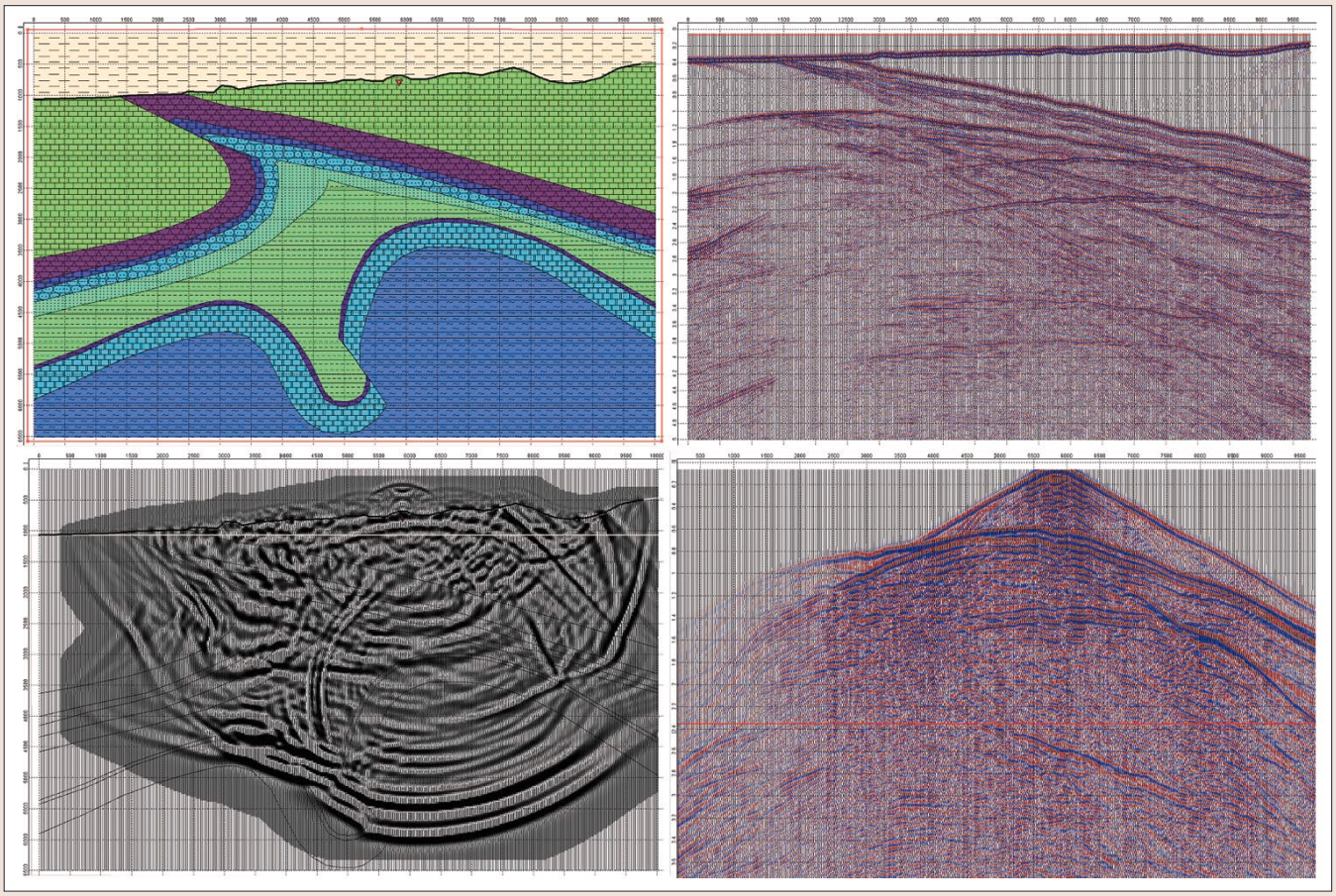

Figure 2. *Modeled shot record. Top left: Grid in X, Z, and velocity. Top right: Plane wave modeled response (unmigrated stack). Bottom left: Wavefield snapshot for single source point. Bottom right: Shot record modeled response. (Courtesy of Tesseral Software)*

traces show variable noise. This is most easily demonstrated when the records are presented on a computer screen and the images are flickered back and forth.

I have performed this test as a part of several hundred vibroseis program start-ups over the years. In most areas, noise that would be considered random when observed on a single record can be demonstrated to be repeatable for a given source location. I propose that this noise is source-generated and is probably a result of scattered surface waves, in particular scattered trapped mode waves (Cooper and O'Neill, 1997). As such, this noise will only be suppressed by stacking provided the stacked traces consist of a variety of source locations and offsets. I often refer to such noise as offset dependent.

In addition, certain types of noise can be attributed to source or receiver locations. This would include local sources of noise such as pump jacks, compressor plants, wet or boggy areas, et cetera. To some extent, some of these types of noise may have a time-variant component as well.

Some types of noise may be azimuth-dependent. We have all seen shot records with a strong air blast to one side of the shot and not to the other side. This can be due to wind direction or some type of shield near the shot such as a cliff or large building. Wind, surface topography, and near-surface geologic anisotropy can contribute to azimuth variant noise.

Design of a seismic survey must include an evaluation of samples of existing data in the project area if they are available. Shot records are best, although common-offset stacks may also help us determine the nature of noise generators. Only in this manner can we make intelligent determinations of required trace densities (or fold).

It is important to ensure that our stacked traces will embrace a broad variety of recording times (as in time of day, not record length), offsets, source locations, receiver locations, and azimuths. A review of existing seismic records will indicate which of these variables may be most important in a certain area. For example, recording through a city (such as Los Angeles, Paris, Tokyo) will require strong weapons against cultural noise (generally random when considered over a long vibroseis sweep). In general, however, truly robust surveys should have a great diversity of all statistics.

Trace density versus fold. The subsurface redundancy obtained for a particular target depends very much on the intersection of the recording patch and a circle defining the useable offsets for that target. In the case of anisotropic muting, the circle would become an ellipsoid.

There are four cases for calculating this intersection. Figure 4 presents the equations used for each case to calculate useable patch area.

Note that the radius of useable offsets (maximum useable offset or X_{max}) is generally determined by the processing mute and will vary with target depth. On larger surveys, the mute will also vary spatially as target depth changes and as velocity fields change.

In 2D survey design, X_{max} is often estimated by a rule of thumb that states that it is approximately equal to the depth of the target. However, 3D grid density is sensitive to X_{max} squared and this value should be considered much more carefully. Grid density will affect both image quality (denser is better) and project cost (sparser is better).

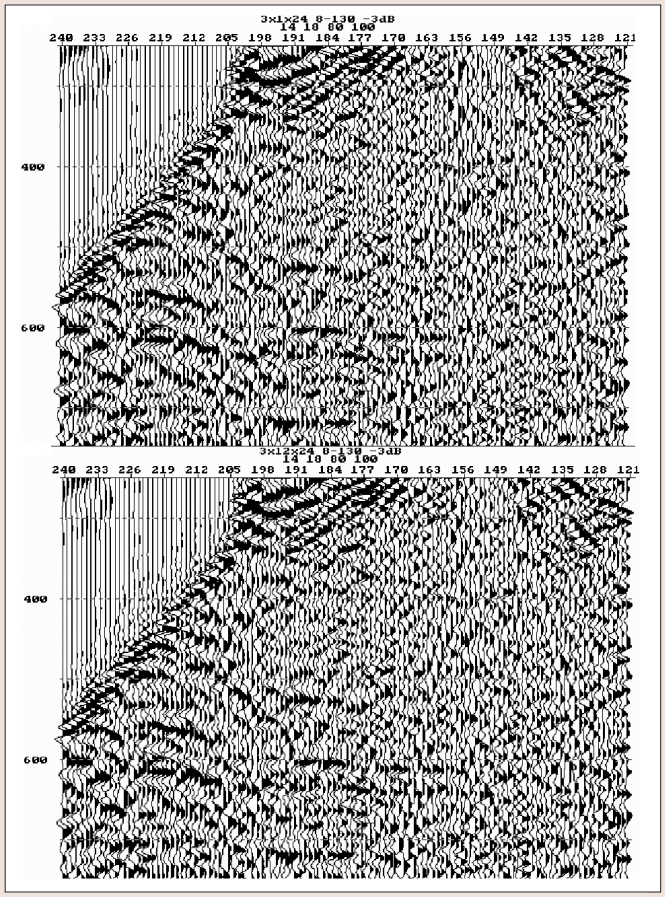

Figure 3. *Two observations of the same source point. The top record was the result of a single sweep using three vibrators. The bottom was recorded about 15 minutes later as the sum of 12 sweeps from the same three vibrators. Vibrators were center stacked in both examples.*

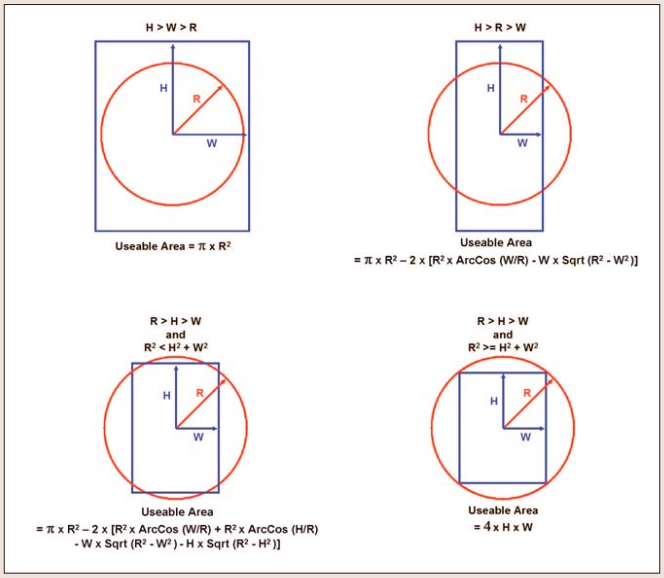

Figure 4. *Intersection of recorded patch with useable offsets. Four relationships can be identified depending on the useable offset (R) versus the half height of the recorded patch (H) and the half width (W).*

Factors affecting X_{max} include:

- depth to target of interest
- the velocities of various contributions to first breaks (including the direct wave and the dominant refractions),
- the amplitude levels of first breaks (for what period of time following the onset of the first break is the data dominated by the energy of the first break?),

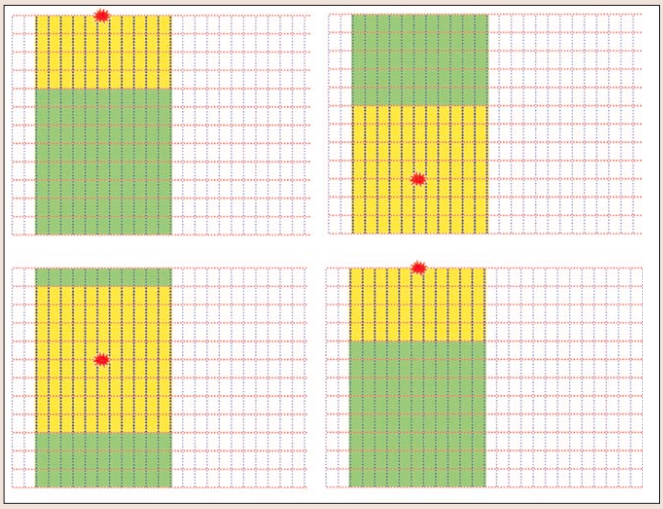

Figure 5. *Receivers required to service a patch. Most recording crews use multiple shooters to acquire data efficiently. The shooters are scattered along the central swath. Depending on which shooter calls in ready, the appropriate patch around him is activated, so they must have enough recording channels to record any part of the receiver lines used in a patch.*

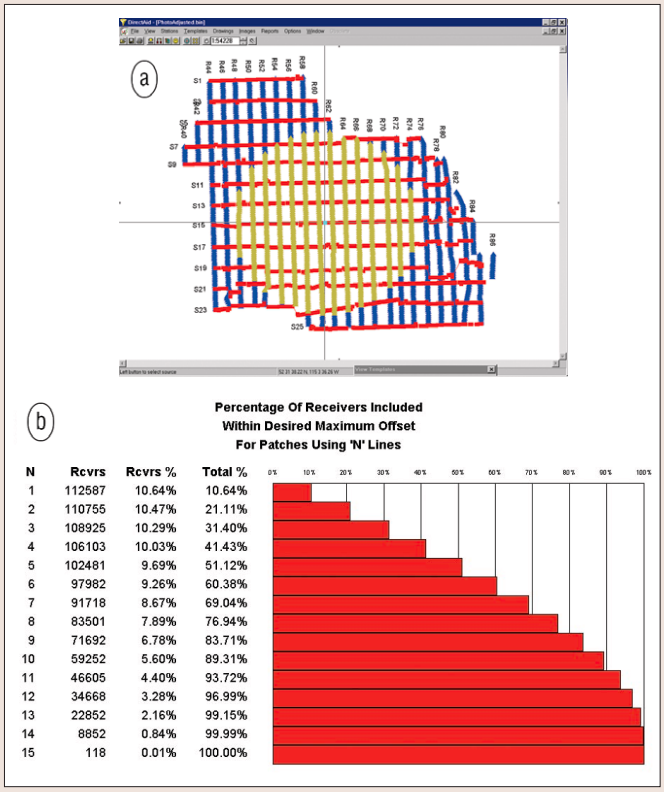

Figure 6. *Patch utilization analysis. First, we shoot the program using a circular patch with a radius of X_{max}. The patches for every shot are analyzed to determine what percentage of traces are captured by the central line only, then the central two lines, then three, et cetera, expanding outwards to the maximum lines available within X_{max}. We see that the outer lines contribute progressively fewer traces and may be considered somewhat optional if equipment limitations become a strong factor. In this example, for the zone and X_{max} considered, we could achieve more than 95% of our desired coverage with a 12-line patch as opposed to 15 lines required to capture absolutely every available trace.*

- NMO stretch mutes,
- deterioration of signal to noise ratio due to spherical divergence and absorption,
- ringing of first breaks due to trapped direct waves and trapped head waves.

Recording patches must be determined through knowledge of field operations and available recording equipment. Keep in mind that for efficient recording operations, receivers must be available along the entire length of recording lines, not just the length of the patch (as shown in Figure 5). Therefore, the crew must maintain sufficient recording channels to lay out all receivers across the survey for each line of the active patch, plus 2-4 additional lines to allow for pick up and layout. The more miles of cable to service and the more channels on the ground, the higher will be the cost of the program. I generally try to moderate this cost by analyzing the optimum patch width for both imaging and operations. Figure 6 summarizes the technique.

Once we have determined the effective X_{max} for our prime zones of interest, we are ready to consider the required grid density. For this, I prefer an accepted version of the 3D fold equation:

$$Fold_{3D} = \frac{\pi X_{\max}^2}{4 \times SL \times RL}$$

where *SL* and *RL* represent average source and receiver line spacing, respectively. Note that this equation delivers the nominal fold as gathered in natural bins (1/2 receiver interval by 1/2 source interval). It also assumes that a full-aperture patch has been recorded (one that embraces at least 100% of all available traces). For more accurate results, the equations from Figure 4 should be used for the numerator if the patch is not full-aperture.

Some idea of our required source and receiver intervals will have been gained by methods described earlier in this paper where wavefield complexity was evaluated. Once we know the surface source or receiver interval that will sample the important characteristics of our expected wavefield without aliasing, then the best imaging will be obtained if the line spacing equals the source and receiver interval. This would result in a "full wavefield" 3D as depicted in the left portion of Figure 7.

The advantage of the full wavefield design is that every subsurface bin will contain traces of every possible offset, and that the offset and azimuth distribution of each bin will be identical to all other bins. There will be no bin-to-bin inhomogeneity to produce variable stacking characteristics.

When we enlarge the box (increase source and receiver line spacing), we create more bins within each box. In particular, consider one quadrant of a box. In the full wavefield design, every offset appears in each quadrant (left of Figure 8). This is also true of the sparser orthogonal design on the right of Figure 8. However, with a sparser grid, we have more natural bins amongst which to share these offsets, resulting in some bin-to-bin heterogeneity and the appearance of what we refer to as "geometric noise" in the data.

When we choose not to record many of the lines dictated by full wavefield sampling, we inherently increase the area of responsibility for each source and receiver in the survey. This leads to the concept of surface source and surface receiver bins (Figure 9) and ultimately to the principles of skidding and offsetting guidelines. I recommend a guideline such as that depicted in Figure 10 in which the first choices for alternate source locations are within one surface source bin. In the field, we should provide several alternatives for the surveyors to choose from. Their eyes in the field will provide the best information as to which of these choices are the most feasible from an operational standpoint.

Obviously, few (if any) companies can afford the full wavefield 3D design as a standard operating design. As program designers, our concern becomes, "How sparsely can we approximate the full wavefield model and still achieve our objectives?"

For many geophysicists, "meeting our objectives" means attaining a certain desired fold. To determine grid density, we simply rearrange the above fold equation to:

$$SL \times RL = \frac{\pi X_{\max}^2}{4 \times Fold_{Desired}}$$

If the sparseness coefficients (M and N in Figure 7) are small, then I agree with Vermeer's contention that *SL* and *RL* should be equal. However, for larger sparcities, I believe this criterion becomes less important. I encourage the designer to use the aspect ratio (*SL/RL*) to maximize operational efficiency and cost. For imaging purposes, I suggest that the aspect ratio be maintained in the range:

$$\frac{2}{3} \le \frac{SL}{RL} \le \frac{3}{2}$$

and only under rare circumstances should it be allowed to violate:

$$0.5 \le \frac{SL}{RL} \le 2.0$$

Note that for any given box area ($SL \times RL$), an aspect ratio of 1:1 will result in the minimum linear kilometers of trail (box perimeter). However, the cost per km for source trails with source points is often greater than the cost of receiver trails and receiver points. Therefore, an aspect ratio somewhat larger than 1:1 will be most efficient. Given that source trails are generally wider than receiver trails, this will also reduce environmental impact.

I am often faced with comparing the characteristics of one design to another. If the two designs entertain different bin dimensions, then this comparison can result in some misleading conclusions.

I am not fond of the common practice of using fold in natural bins as a yardstick of design quality and suggest the use of trace density. To obtain this, simply calculate the useable area of the recording patch for the zone of interest (as per Figure 4), multiply by 10^6 (to make units of per square kilometer) and divide by the product of $SL \times RL \times Si \times Ri$ (source line spacing times receiver line spacing times source interval times receiver interval). Notice that this is the same as nominal fold divided by the area of a natural bin. Trace density is significant because it represents the number of traces per square kilometer within the selected mute (or X_{max}) that will image the target.

$$Trace\ Density = \frac{(useful\ area\ of\ patch) \times 10^6}{4 \times SL \times RL \times (Si/2) \times (Ri/2)}$$

The suggested calculations normalize fold by bin area. If desired, further multiplication by the migration operator area (in km^2) gives the trace density within the migration operator. This is similar to the concept of "point cloud density" in light detection and ranging (Lidar) imaging. Depending on your comfort with small numbers, you may want to eliminate the factor of 10^6 and consider the fractional number of "traces per square meter" which results. As an example, consider a survey with 60-m source and receiver intervals, 240-m *RL* and 360-m *SL*. Assume that offsets of 0-1500 m are useable at the zone of interest and that the patch will be large enough to record all such offsets. Then:

$$Fold_{3D} = \frac{\pi \times (1500)^2}{4 \times 360 \times 240} = 20.45$$

$$Trace\ Density = \frac{\pi \times (1500)^2 \times 10^6}{SL \times RL \times Si \times Ri} = 22\ 725.64\ traces\ per\ km^2$$

or 0.0227 traces per m^2
or one trace per 44 m^2
or one trace per 6.6 by 6.6 m

Provided that the survey statistics (including midpoint scatter) are sufficiently diverse, then the last number represents the potential spatial resolution of a broadband prestack migration. Of course, limits in our recorded bandwidth usually prevent us from attaining such a resolution.

The targeted number of traces per square kilometer will be determined by the geologic nature of the objective (including depth and stratigraphic or structural complexity) and by the signal to noise conditions in the project area. I recommend the following general guidelines for traces per km^2:

< 6000	generally not advisable
6000 - 18 000	okay for simple structure plays with good *S/N*
18 000 - 25 000	for stratigraphic and subtuning plays with good *S/N*
25 000 - 100 000	increasing as *S/N* deteriorates
25 000 - 100 000	increasing as structural complexity increases

Of course, these numbers assume that the selected 3D designs generate good statistical diversity amongst the traces contributing to the specified density.

Statistical diversity. The discussion of noise earlier in this article emphasized that noise is a function of time of day, source-receiver offset, source location, receiver location, and source-receiver azimuth. Of these factors, time-variant noise is often dominant only in highly populated areas (passing through cities, along major highways). In most other areas, our big noise problems are often due to offset-variant noise (such as scattered trapped modes).

The principle of superposition (Figure 11) indicates that we may enhance signal to noise ratios by a factor equal to the square root of the number of traces averaged. The superposition principle is based on the assumption that the signal is the same on each contributing trace and that the noise does not correlate from trace to trace. If components of the noise are repeatable from trace to trace, then the suppression of noise will be less effective. When we stack our data, we are attempting to stabilize our reflectivity estimates by superposition. If our traces are not diverse in all variables affecting noise, then we will not optimize the power of stacking. Indeed, with high levels of redundancy, stacking will provide very little benefit.

Notice that the concept of bin size comes into play only when we stack our data. At that time, we lay a bin grid over the midpoint scatter plot and collect all traces whose midpoints fall within a given bin. These traces are then averaged and a single stacked trace is output for each bin. This product may then be poststack migrated.

If the selection of bin size is sufficient to avoid aliasing of all dip elements and diffractions of geologic interest, then geometric scatter of midpoints across the bin cannot be detrimental to image quality. In fact, uniform scatter of midpoints will provide a spatial antialias filter when reducing field traces to stacked traces. Some geophysicists express concerns about "smearing" geology by allowing midpoint scatter within each bin. If this is a concern, then surely their selected bin size is too large for the expected wavefield complexity.

I regard midpoint scatter as yet another contribution to statistical diversity. I encourage implementation of midpoint scatter by choice of survey design type as well as encouraging natural perturbation of lines (according to established guidelines) during survey implementation.

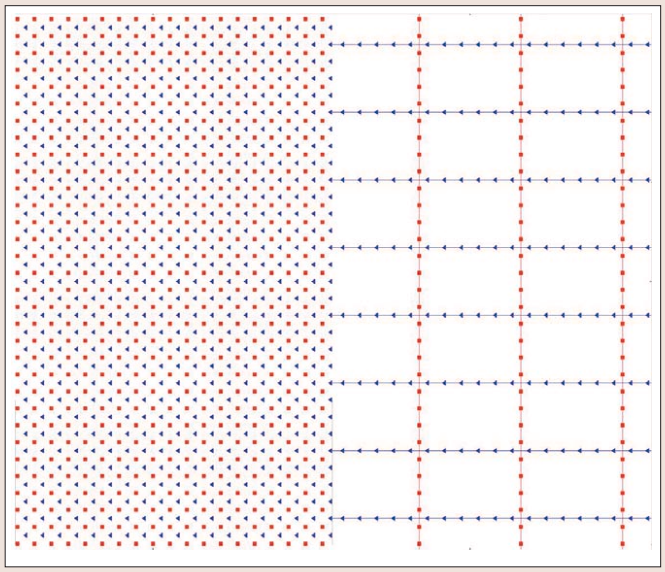

Figure 7. *Full wavefield sampling versus sparse orthogonal sampling. A typical orthogonal survey is simply a sparse approximation to full wavefield sampling. We refer to "M by N" sparseness, in this case using only every fourth receiver line and every sixth source line yields a 4 × 6 sparseness.*

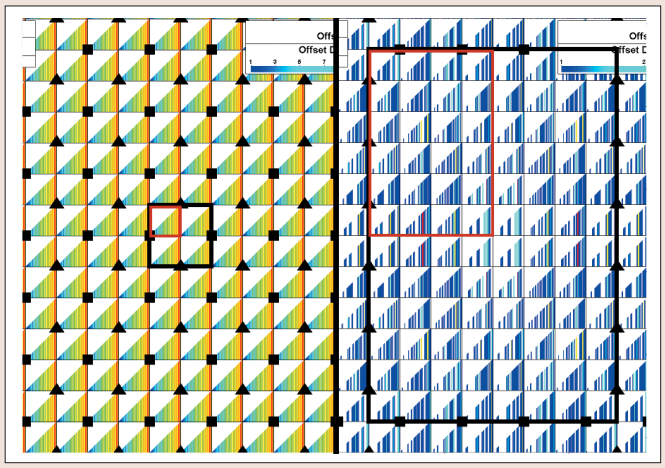

Figure 8. *Full wavefield sampling versus sparse orthogonal sampling - offset distributions. The black outlines represent one unit "box." This is the area bounded by two adjacent source lines and two adjacent receiver lines. The red outlines indicate one quadrant of each of the respective boxes. For each bin, the distribution of the vertical lines represents the offset contributions for each offset range (increasing from left to right). The color indicates the number of traces of similar offsets for each range (blue to red is 1-21 for the left and 1-4 for the right). Although each bin in a sparse 3D survey contains different offset combinations, notice that all offsets are represented in one quadrant of a box. In other words, if the bin size were set to a quadrant of a box, we would observe complete offset sampling in each bin with no bin-to-bin heterogeneity.*

However, I strongly encourage the use of prestack migration (at least prestack time migration). During prestack migration, the bin grid is not used to collect traces. In fact, all traces within the migration operator are weighted and summed to a single output location. In this case, midpoint scatter has the potential to truly increase spatial resolution. Of course, we must specify an output trace interval for the migration process, but this need not be related to the natural bin size.

Ultimately, the following factors may limit our ability to image spatially small reflection elements of targets:

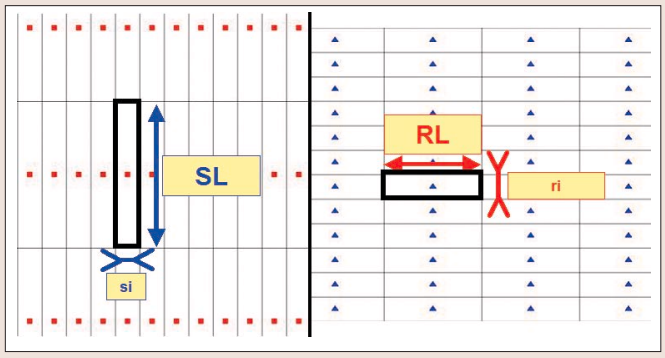

Figure 9. *Surface bins for sources (left) and receivers (right). The area of responsibility for each source and receiver is increased when we choose a sparse orthogonal design. SL and RL refer to source and receiver line spacing, respectively; si and ri refer to source and receiver intervals along each line.*

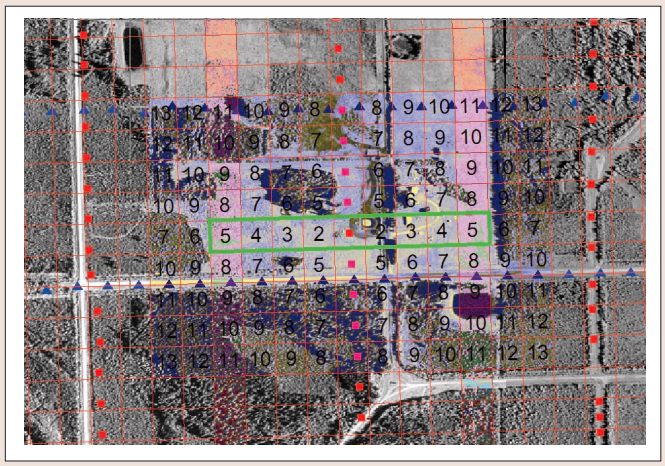

Figure 10. *Skid and offset guidelines. A grid of "surface bins" (each bin being one source interval by one receiver interval in size) is centered on a source point that needs to be relocated. The grid is oriented parallel to receiver lines. The number in each cell of this "bingo card" represents the order of preference for a source location. The most preferred locations (numbers 1-5) are defined within the surface source bin corresponding to the source being moved (indicated by the green outline). Other choices should be considered only if choices within the green rectangle are not feasible.*

Figure 11. *Principle of superposition. Averaging N traces produces a $N^{1/2}$ improvement in signal to noise ratio.*

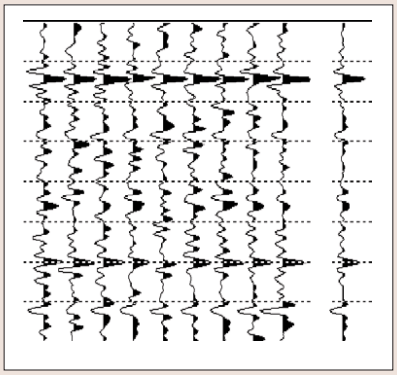

- Geologic complexity. Structural dips or diffractions from lateral velocity changes must exist. If the geology does not contain lateral velocity or density changes then, of course, we will have nothing to resolve.
- Recoverable bandwidth. The final processed bandwidth at the target zone will not only determine the limit of vertical resolution (often stated as a quarter wavelength) but will also form one limit on spatial resolution (sometimes stated as a half wavelength:

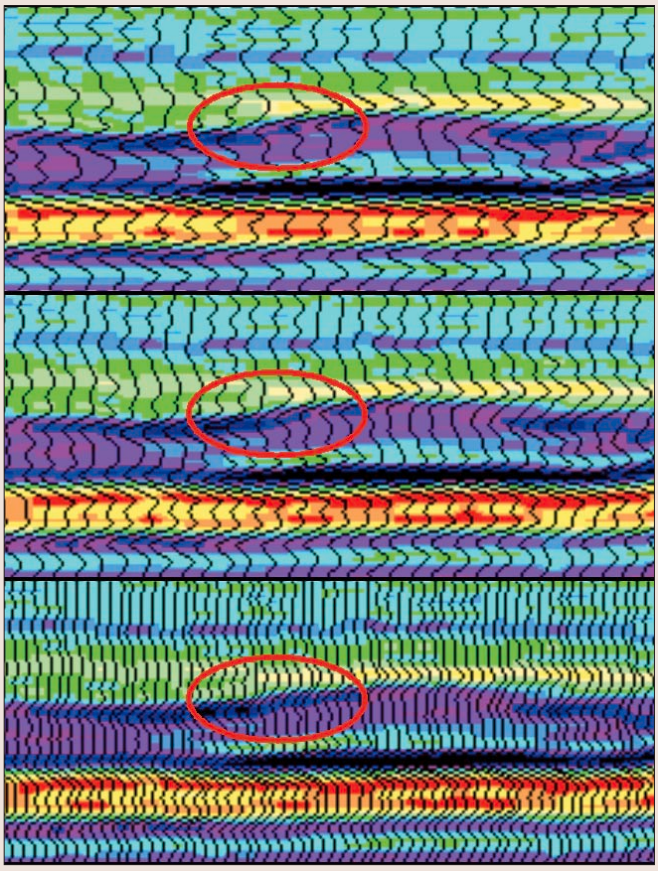

Figure 12. *Testing PSTM output trace interval. This is an example from a shallow steam flood project. Each panel is only 50 ms of data. The top panel was prestack time migrated to a 12-m bin (natural bin size), the middle panel to an 8-m bin and the bottom panel to a 4-m bin. Frequencies up to 140 Hz were included and the average velocity to the target is 2000 m/s. This would lead us to expect potential spatial resolution of about 7.1 m. Note that migration to 8-m bins provides a steeper image of the front of the steam chamber compared to the 12-m bins. Reducing output trace spacing from 8 to 4 m delivers more traces but does not significantly sharpen the image.*

$$\frac{1}{2}\lambda = \frac{Velocity}{2 \times Frequency}$$

- Output trace spacing after migration (as per Nyquist).

Our job is to ensure that the output trace spacing does not impose more restrictive limits than those imposed by the first two factors. It would be wasteful of processing time and processing budget to output more traces than necessary to meet the limits of the first two factors. I recommend testing output bin size on a small data cube. The results of one such test are presented in Figure 12.

Note that if midpoints are tightly focused at natural bin centers, then there is no diversity in the input spatial grid and resolution below that of the natural bin size should not be expected. On the other hand, with maximum midpoint scatter, resolution is potentially achievable to the individual trace area (6.6 × 6.6 m in our previous trace density example). Of course, midpoint scatter alone cannot ensure spatial resolution without sufficient bandwidth and geologic complexity.

One last word on statistical diversity: While offset and azimuth distribution along with source and receiver locations are obvious, statistics that require diversity within each bin gather, it has been demonstrated that midpoint scatter also contributes to diverse sampling. On a more subtle level, box aspect ratio is also a contributor to statistical diversity in the

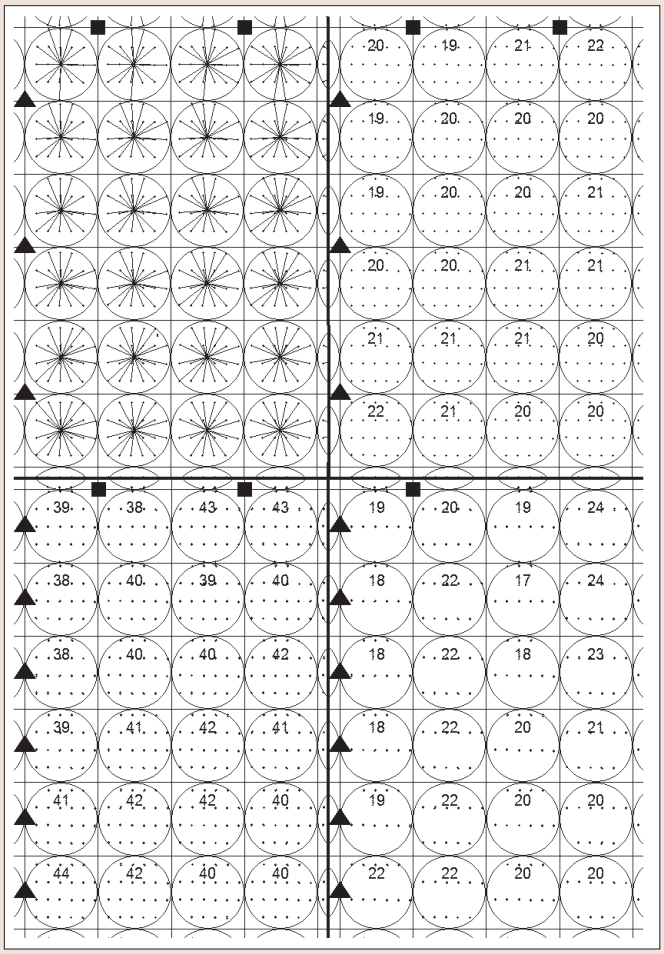

Figure 13. *Source density versus receiver density. In the top left is a conventional "spider plot" for one 3D model. In the top right, the vectors have been removed and only the polar coordinates retained for each trace in each bin. The bottom left depicts the same 30-m bins but using a 30-m receiver interval. In the bottom right, every second shot has been removed.*

case of sparse surveys (Cooper and Herrera, 2002). Provided the sparseness indices *M* and *N* are not very small, some statistical distributions benefit from a moderate box asymmetry. This supports the earlier recommendation to consider some asymmetry in order to optimize survey costs and operations.

The tools of our trade: an example where fold can be misleading. I have been asked on a number of occasions about a proposal to reduce costs by increasing the number of receivers along each line and decreasing the number of sources. Provided the survey is gathered in the natural bins for the original parameters, fold will be invariant. While this is true, I strongly discourage this practice as it disregards diversity of offsets and azimuths.

Figure 13 depicts such an example. In the top left is a conventional spider diagram for a survey using 60-m source and receiver intervals, 240-m receiver line spacing, and 360-m source line spacing. The survey was recorded with a wide aperture patch sufficient to record all offsets within 1500 m and was then offset limited to 1500 m.

Notice that a spider plot is actually a polar plot within each bin showing offset as a vector from the center of the bin to an outer circle at the maximum offset limit. The azimuth of the vector indicates the source-receiver azimuth. I find that it is better to view this plot without the vector lines and plot only a point at the tips of the vectors to represent the polar coordinate of each trace (top right of Figure 13). I have also noted the total fold for each bin.

The bottom left plot shows the effect of doubling the number of receiver points along each receiver line (receiver interval is decreased to 30 m, but I still use 30 × 30 m bins). Notice that although the fold is doubled, this practice results in a pairing of each offset-azimuth coordinate. Each adjacent pair of receivers produces nearly redundant coordinates within the original bins.

The bottom right plot of Figure 13 completes the proposed strategy by removing half of the sources from each source line. From line to line, I alternated removing odd and even sources to produce a checkerboard effect. Notice that the distribution of statistics is reduced. Although fold is very similar in the two plots on the right, the offset-azimuth statistics are much better distributed on the original (top plot).

This example underscores a fundamental design concept. Once we have determined the required source and receiver intervals that avoid aliasing of key reflection elements, we gain very little by creating designs with smaller intervals. In fact, we reduce survey efficiency and increase costs.

This brings up a question that is commonly asked. With recording systems such as the Schlumberger Q system or the Vibtech "it System" now offering virtually unlimited recording channels, how can we make good use of tens of thousands of channels? Similarly, we have efficient new sources such as Polaris' new "hammer" which is capable of initiating source points at a rapid rate for a low cost.

The previous example illustrates that there is generally little value in producing more source points or receivers along typical grid spacing. In order to truly benefit from increased source or receiver capacities, we must be able to reduce line spacing in an environmentally friendly and cost-effective manner.

There are areas where this may be feasible (such as open desert or farm land where fences and permit fees are a minimum). But for most applications on land, our next challenge will be to reduce the cost and impact of tight 3D grids. Such methods as mulcher cutting of forested areas, combination of LIDAR with GPS, and integrated navigation system surveys, block permitting, and nonintrusive methods will allow us to increase the density of seismic surveys.

Summary. A summary of this tutorial will appear at the end of Part 2, which will appear in November's *TLE*.

Appendix - some useful calculations.

Offset where direct wave interferes with reflection. Equation for reflection hyperbola:

$$t_x = \sqrt{t_0^2 + \frac{x^2}{V_{rms}^2}} \tag{1}$$

Equation for muted direct wave:

$$t_x = \frac{x}{V_{direct}} + Mute \tag{2}$$

By equating (1) and (2) we can solve for the offset of intersection:

$$\sqrt{t_0^2 + \frac{x^2}{v_{rms}^2}} = \frac{x}{V_{direct}} + Mute$$

Solving for x yields:

$$x = \frac{-b \pm \sqrt{b^2 - 4ac}}{2a}$$

where:

$$a = \left(\frac{1}{V_{rms}^2} - \frac{1}{V_{direct}^2} \right)$$

$$b = -\left(\frac{2\ Mute}{V_{direct}} \right)$$

$$c = t_0^2 - Mute^2$$

The same derivation applies to interference with a refracted wave with the following modifications:

- substitute $V_{refractor}$ for V_{direct}
- the mute should include the intercept time for the refraction

Offset of sufficient NMO for velocity analysis. Equation for reflection hyperbola:

$$t_x = \sqrt{t_0^2 + \frac{x^2}{V_{rms}^2}}$$

At what offset does t_x - t_0 = P, where P is 1.5 times the dominant period of the data?

$$\sqrt{t_0^2 + \frac{x^2}{V_{rms}^2}} - t_0 = P$$

Solving for x yields:

$$x = \sqrt{V_{rms}^2\ (P^2 + 2\,P\,t_0)}$$

The same derivation applies to the calculation of sufficient NMO for multiple cancellation with the following modifications:

- substitute $V_{multiple}$ for V_{rms}
- P should be 3.0 times the dominant period of the data

Offset where NMO stretch limit first occurs. Normal moveout corrections are applied to data in the course of processing. Since this is a dynamic process, the correction applied at one point in time is not the same as the correction applied at a different point in time (except at the zero-offset trace). This results in a stretching of data that distorts wavelet characteristics. Most NMO programs mute data that is stretched more than a specified percentage. This percentage can be specified as the difference in moveout corrections for two points divided by the original separation of those two points. A formula for NMO stretch at a point is derived by taking the limit of this ratio as the time separation of the two events approaches zero. Expressed as a percent this is of the form:

$$\%\ Stretch = -100 * \lim_{t \to t_0} \left(\frac{F(t_0) - F(t)}{G(t_0) - G(t)} \right)$$

where:

$$F(t_0) = \left(\sqrt{t_0^2 + \frac{x^2}{V_{rms}^2}} - t_0 \right)$$

and:

$$G(t_0) = \left(\sqrt{t_0^2 + \frac{x^2}{V_{rms}^2}} \right)$$

Or:

$$\%\ Stretch = -100 * \lim_{t \to t_0} \left(\frac{F(t_0) - F(t)}{t_0 - t} * \frac{t_0 - t}{G(t_0) - G(t)} \right)$$

which we recognize as:

$$\%\ Stretch = -100 * \left(\frac{\frac{d}{dt} F(t_0)}{\frac{d}{dt} G(t_0)} \right)$$

Taking the derivatives of $F(t_0)$ and $G(t_0)$ and solving for x yields:

$$x = t_0 * V_{rms} * \sqrt{\left(1 + \frac{\%\ Stretch}{100} \right)^2 - 1}$$

Aliasing of structural/stratigraphic dips. A CDP stacked section will exhibit wavenumber aliasing of data that are sampled with less than two traces per apparent wavelength.

The following derivation is for a plane wave and only considers one-way traveltime. (Allowance for two-way traveltime would reduce the outcome by a factor of two.) For basins where velocity generally increases with depth, curved ray theory tends to compensate for this oversight. Furthermore, this derivation is generally consistent with measurements made from real seismic data. It also is supported by several decimation tests performed on data in the Western Canadian Basin.

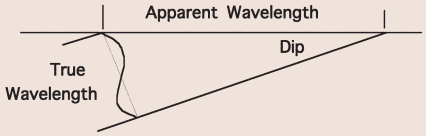

Assuming plane wave theory, the shortest true wavelength of a reflection is:

$$Wavelength = \frac{V_{average}}{Freq_{maximum}}$$

The shortest apparent wavelength of a dipping reflection is:

$$Apparent\ Wavelength = \frac{V_{average}}{Sin(Dip)\ Freq_{maximum}}$$

and the largest unaliased spatial sample interval is:

$$Interval_{dip} = \frac{a \times V_{average}}{b \times Sin(Dip)\ Freq_{maximum}}$$

where:

a = 1 for subsurface (bin size) and 2 for surface (receiver interval) size
b = 2 to meet minimum Nyquist requirements
b = 3 is safer in presence of noise and statics. This also provides for a safety margin.

Suggested reading. "A review of some 3D and 2D models using data simulation" by Cooper and Herrera (presented at 2002 CSEG National Convention). "Trapped mode and guided waves—a common noise problem" by Cooper and O'Neil (presented at 1997 CSEG National Convention). *3D Symmetric Sampling* in Theory and Practice by Vermeer (*TLE*, 1998). TLE

Corresponding author: ncooper@mustagh.com